

Prediction and Communication Co-design for Ultra-Reliable and Low-Latency Communications

Zhanwei Hou, Changyang She, Yonghui Li, Zhuo Li, and Branka Vucetic

Abstract

Ultra-reliable and low-latency communications (URLLC) are considered as one of three new application scenarios in the fifth generation cellular networks. In this work, we aim to reduce the user experienced delay through prediction and communication co-design, where each mobile device predicts its future states and sends them to a data center in advance. Since predictions are not error-free, we consider prediction errors and packet losses in communications when evaluating the reliability of the system. Then, we formulate an optimization problem that maximizes the number of URLLC services supported by the system by optimizing time and frequency resources and the prediction horizon. Simulation results verify the effectiveness of the proposed method, and show that the tradeoff between user experienced delay and reliability can be improved significantly via prediction and communication co-design. Furthermore, we carried out an experiment on the remote control in a virtual factory, and validated our concept on prediction and communication co-design with the practical mobility data generated by a real tactile device.

Index Terms

Ultra-reliable and low-latency communications, prediction and communication co-design, delay-reliability tradeoff

Part of the work has been presented in IEEE international communications conference (ICC) 2019 [1].

Z. Hou, C. She, Y. Li and B. Vucetic are with the School of Electrical and Information Engineering, University of Sydney, Sydney, NSW 2006, Australia (email: {zhanwei.hou, changyang.she, yonghui.li, branka.vucetic}@sydney.edu.au). Z. Li is with Beijing University of Technology, Beijing, China (email: zhuoli@bjut.edu.cn).

I. INTRODUCTIONS

A. Backgrounds and Motivations

Ultra-reliable and low-latency communications (URLLC) are one of the new application scenarios in 5G communications [2]. By achieving ultra-high reliability (e.g., 10^{-5} to 10^{-8} packet loss probability) and ultra-low end-to-end (E2E) delay (e.g, 1 ms), URLLC lays the foundation for several mission-critical applications, such as industrial automation, Tactile Internet, remote driving, virtual reality (VR), and tele-surgery [3–5]. How to achieve two conflicting requirements on delay and reliability remains an open problem.

To improve reliability, several technologies have been proposed in the existing literature and specifications, such as K-repetition [6], frequency hopping [7], large-scale antenna systems [8], and multi-connectivity [9]. With these technologies, different kinds of diversities are exploited to improve reliability at the cost of more radio resources. On the other hand, to reduce latency in the air interface, the short frame structure was proposed in 5G New Radio (NR) [10], and fast uplink grant schemes were proposed to reduce access delay [11, 12]. However, there are some other delay components in the networks, such as delays in buffers of devices, computing systems, backhauled, and core networks. As a result, the user experienced delay can hardly meet the requirements of URLLC. Novel concepts and technologies that can reduce the user experienced delay and improve overall reliability (i.e., total packet losses and errors in different parts of the system) are in urgent need.

To tackle these challenges, we aim to meet the requirements of URLLC by jointly optimizing prediction and communication. The basic idea is to predict the future system states at the transmitter, such as locations and force feedback, and then send them to the receiver in advance. In this way, the user experienced delay can be reduced significantly. For example, if the E2E delay is 10 ms and the prediction horizon is 9 ms, then the user experienced delay is 1 ms. However, predictions are not error-free, and long prediction horizon will lead to a large prediction error probability. Intuitively, there is a trade-off between the user experienced delay and the overall reliability. To satisfy the two conflicting requirements of URLLC, we need to jointly optimize the prediction and communication systems. Specifically, in this paper, we will address the following questions: 1) *how to characterize the tradeoff between user-experienced delay and overall reliability with prediction and communication co-design?* 2) *Is it possible to satisfy the requirements of URLLC by prediction and communication co-design?* 3) *If yes, how to maximize*

the number of URLLC services that can be supported by the system?

The above questions are challenging to answer since multiple components of delay and errors are involved in prediction and communication systems. As such, we need a prediction and communication co-design framework which takes different delay components and errors into account. Moreover, the complicated constraints on the user experienced delay and the overall reliability are non-convex in general, and hence it is very difficult to find the optimal solution.

B. Our Contributions

The main contributions of this paper are summarized as follows:

- We establish a framework for prediction and communication co-design, where the time and frequency resource allocation in the communication system and the prediction horizon in the prediction system are jointly optimized to maximize the number of devices that can be supported in the system.
- We derive the closed-form expressions of the decoding error probability, the queueing delay violation probability, prediction error probability, and analyzed their properties. From these results, the tradeoff between user experienced delay and overall reliability can be obtained.
- We propose an algorithm to find a near optimal solution of the optimization problem. The performance loss of the near optimal solution is studied and further validated via numerical results. Besides, we analyze the complexity of the algorithm, which linearly increases with the number of devices.

Furthermore, to evaluate the performance of the proposed method, we compared it with a benchmark solution without prediction. Simulation results show that the tradeoff can be improved remarkably with prediction and communication co-design. In addition, an experiment is carried out to validate the accuracy of mobility prediction in practical remote-control scenarios.

The rest of this paper is organized as follows: In Section II, we review the related literature. The system model is presented in Section III. The co-design of prediction and communication is proposed in Section IV. Numerical and experimental results are presented in Section V, and conclusions are drawn in Section VI.

II. RELATED WORK

A. *Communications in URLLC*

There are some existing solutions to reduce latency in communication systems for URLLC [10–14]. With the 5G New Radio (NR) [10], the notion of “mini-slot” is introduced to support transmissions with the delay as low as the duration of a few symbols. The queueing delay is analyzed and optimized in [13], where the tradeoff among throughput, delay and reliability was studied. To reduce the access delay in uplink transmissions, a semi-persistent scheduling (SPS) scheme was developed in [11]. A grant-free protocol was proposed in [12] to further avoid the delay caused by scheduling requests and transmission grants. With the preemptive scheduling scheme in [14], the short packets with high priority can preempt an ongoing long packet transmission without waiting for the next scheduling period. With this scheme, the scheduling delay of short packets is reduced.

To improve the reliability for the low latency communications, different kinds of diversities were introduced [6–9]. In [6], K-repetition was proposed to avoid retransmission feedback. The basic idea is to send multiple copies of each packet without waiting for the acknowledgment feedback. Considering that the required delay is shorter than channel coherence time, frequency hopping was adopted in [7] to improve reliability. In [8], a Lyapunov optimization problem was formulated to improve the reliability with guaranteed latency, where spatial diversity was used to improve reliability. In [9], interface diversity was proposed to achieve URLLC without modifications in the baseband designs by providing multiple communication interfaces. However, by introducing diversities, the reliability is improved at the cost of low resource utilization efficiency.

This tradeoff between delay and reliability has been exhaustively studied in communication systems [15–18]. To reduce the transmission delay, the blocklength of channel codes is short, and the decoding error probability is nonzero for arbitrary signal-to-noise ratio (SNR). The fundamental tradeoff between transmission delay and decoding error probability in the short blocklength regime was derived in [15]. The tradeoff between the queueing delay and the delay bound violation probability was studied in [16]. To achieve a lower delay bound, the violation probability increases. Moreover, grant-free schemes can help reduce latency, but introduce extra packet losses due to transmission collisions. How to achieve ultra-high reliability with grant-free schemes was studied in [18] and it is shown that the proposed stop-and-wait protocol can achieve

10^{-5} outage probability.

B. Predictions in URLLC

To achieve satisfactory delay and reliability in URLLC, different kinds of predictions have been studied in the existing literature [19–24].

In [19], the predicted control commands were sent to the receiver and waiting in the buffer. When a control command is lost in communications, predicted commands in the receiver’s buffer will be executed. The length of predictive control commands was optimized to minimize the resource consumption. The idea of model-mediated tele-operation approach was mentioned in [20]. By predicting the movement or the force feedback, the user experienced delay can be reduced. In both [19] and [20], prediction errors were not considered, and whether we can achieve ultra-high reliability in the systems remains unclear.

Different from command or mobility predictions in control systems, predicting some other features of traffic or performance of communications is also helpful. In [21], based on the predicted traffic state, a bandwidth reservation scheme was proposed to improve the spectral efficiency of URLLC. By exploiting the correlation among different nodes, the behavior of different users can be predicted [22]. Then, by reserving resources according to the predicted behavior, the access delay can be reduced. A fast hybrid automatic repeat request (HARQ) protocol was proposed in [23], prediction is used to omit some HARQ feedback signals and successive message decodings, so that the expected delay can be improved by 27% to 60% compared with standard HARQ. In [24], the outcome of the decoding was predicted before the end of the transmission. With the predicted result, there is no need to wait for the acknowledgment feedback, and thus the E2E delay can be reduced.

III. SYSTEM MODEL

As shown in Fig. 1, we consider a joint prediction and communication system, where N mobile devices send packets to a receiver, which could be data center, controller, or tactile device. The function of the receiver depends on specific applications. In remote driving [3], a human driver can remotely control a vehicle based on the feedback from various sensors installed on the vehicle. In factory automation [4], sensors update information to the controller to perform better closed-loop control, or to a data center for monitoring or fault detection. In Tactile Internet [5], force and torques are sent to a tactile device to render the sense of touch,

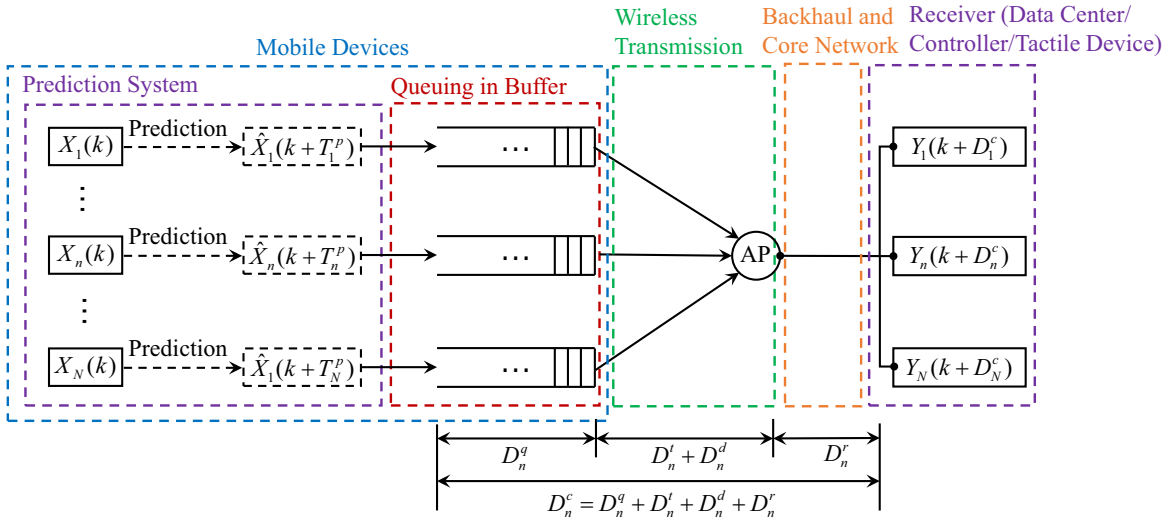


Fig. 1. Illustration of network structure.

and thus can enable haptic communications. The packets generated by each device may include different features, such as the location, velocity and acceleration of a device in remote driving or industrial automation, or the force and torques in Tactile Internet.

The receiver can be deployed at a mobile edge computing (MEC) server or a cloud center. In our framework, we consider a general wireless communication system, where mobile devices send packets to a cloud center via wireless links, backhauls, and core networks. The framework is also suitable for an MEC system, where the delays and packet losses in backhauls and core networks are set to be zero [25].

A. User Experienced Delay

Time is discretized into slots. The duration of each slot is denoted as T_s . Let $X_n(k) = [x_n^1(k), x_n^2(k), \dots, x_n^F(k)]^T$ be the state of the n th device in the k th slot, where F is the number of features. The state of the n th device that is received by the receiver in the k th slot is denoted as $Y_n(k)$. In traditional communication systems, each device sends its current state $X_n(k)$ to the data center. Let D_n^c (slots) be the n th device's end-to-end (E2E) delay in the communication system. If the packet that conveys $X_n(k)$ is decoded successfully in the $(k + D_n^c)$ th slot, then $Y_n(k + D_n^c) = X_n(k)$, and the user experienced delay is D_n^c . For clarification, the key notations are listed in Table I.

where B_n is the bandwidth, P_n^t represents the transmit power, N_0 denotes the noise power spectral density, $\gamma_n = \frac{a_n g_n P_n^t}{\vartheta N_0 B_n}$ represents the received SNR, a_n denotes the large-scale channel

TABLE I
INDEX OF KEY NOTATIONS

Notation	Description
N	number of mobile devices
F	number of features in a state
K_n	number of copies transmitted in K -Repetition
T_s	duration of each time slot
D_n^c	end-to-end(E2E) delay in communication system
D_n^c	end-to-end(E2E) delay in communication system
T_n^p	prediction horizon of the n th device
D_n^e	delay experienced by the n th device
D_n^q	queueing delay of the n th device
D_n^t	transmission delay of the n th device
D_n^d	decoding delay of the n th device
D_n^r	delay in backhauled and core networks of the n th device
D_n^τ	transmission duration of each copy in K -Repetition of the n th device
D_{\max}	delay requirement
ε_n^p	prediction error probability of the n th device
ε_n^q	queueing delay bound violation probability of the n th device
ε_n^t	packet loss probability of the n th device
ε_n^τ	decoding error probability of the n th device
$\bar{\varepsilon}_n^\tau$	expected decoding error probability of the n th device
ε_n^o	overall reliability of the n th device
ε_{\max}	reliability requirement
$X_n(k)$	state of the n th device in the k th slot
$\hat{X}_n(k)$	predicted state of the n th device in the k th slot
$Y_n(k)$	received state of the n th device in the k th slot
$W_n(k)$	transition noise of the n th device in the k th slot
$E_n(k)$	difference between real state and predicted state of the n th device in the k th slot
Φ_n	state transition matrix of the n th device
E_n^B	effective bandwidth of the n th device
λ_n	average packet arrival rate of the n th device
B_n	bandwidth of the n th device
η	fraction of time and frequency resources for data transmission
P_n^t	transmit power of the n th device
N_0	noise power spectral density
γ_n	SNR of the n th device
a_n	large-scale channel gain of the n th device
g_n	small-scale channel gain of the n th device
ϑ	SNR loss due to inaccurate channel estimation
$f_Q^{-1}(\cdot)$	inverse function of the Q-function
N_r	number of antennas at the AP

gain, g_n is the small-scale channel gain, $\vartheta > 1$ is the SNR loss due to inaccurate channel estimation, $V_n = 1 - [1 + \gamma_n]^{-2}$ [15], $f_Q^{-1}(\cdot)$ is the inverse function of the Q-function, and ε_n^τ is the decoding error probability. The blocklength of channel codes is $\eta D_n^\tau T_s B_n$. When the blocklength is large, (2) approaches the Shannon capacity.

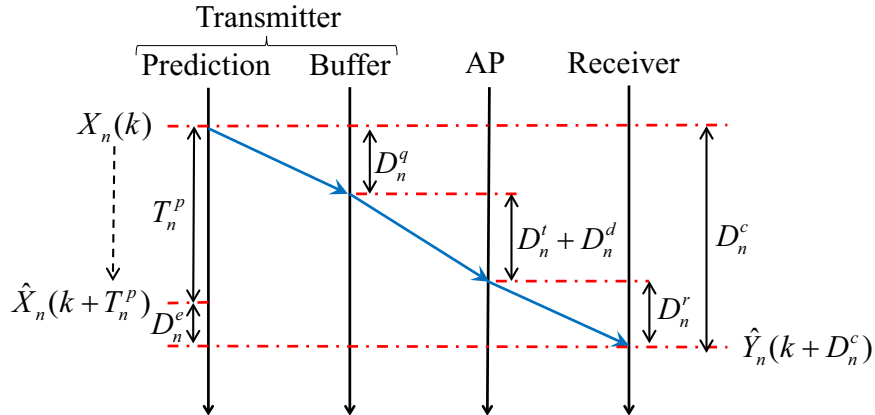


Fig. 2. Illustration of prediction and communication co-design.

As shown in Fig. 2, to improve the user experienced delay, each device predicts its future state. T_n^p is denoted as the prediction horizon. In the k th slot, the device generates a packet based on the predicted state $\hat{X}_n(k + T_n^p)$. After D_n^c slots, the packet is received by the data center. Then, we have $Y_n(k + D_n^c) = \hat{X}_n(k + T_n^p)$, which is equivalent to $Y_n(k) = \hat{X}_n[k - (D_n^c - T_n^p)]$, $\forall k$. Therefore, the delay experienced by the user is $D_n^e = D_n^c - T_n^p$.¹

Remark 1. It is worth noting that the states of adjacent slots could be correlated. Thus, source coding schemes that compress the information in multiple slots can achieve higher compression ratio. On the other hand, channel coding schemes that encode the packets to be transmitted in multiple slots into one block, can achieve higher reliability. However, both of them will lead to a longer decoding delay. To achieve ultra-low latency, in this paper we assume that the source coding and channel coding in the k th slots only depend on $\hat{X}_n(k + T_n^p)$ and the data to be transmitted in this slot.

¹If D_n^c is smaller than T_n^p , D_n^e is negative. This means that the receiver can predict the states of devices. In this paper, we only consider the scenario that $D_n^e \geq 0$.

B. Delay and Reliability Requirements

The delay and reliability requirements are characterized by a maximum delay bound and a maximum tolerable error probability, D_{\max} and ε_{\max} . It means that $X_n(k)$ should be received by the data center before the $(k + D_{\max})$ th slot with probability $1 - \varepsilon_{\max}$.

To satisfy the delay requirement, the user experienced delay should not exceed a maximal delay bound, i.e.,

$$D_n^e = D_n^c - T_n^p \leq D_{\max}. \quad (1)$$

In the considered communication system, the E2E communication delay D_n^c includes queuing delay D_n^q , transmission delay D_n^t , decoding delay D_n^d , and delay in backhubs and core networks D_n^f .

Thus, the constraint in (1) can be re-expressed as follows,

$$D_n^q + D_n^t + D_n^d + D_n^f - T_n^p \leq D_{\max}, \quad (2)$$

where $D_n^d = \kappa D_n^t$, $\kappa > 0$.

The overall reliability depends on prediction errors and packet losses in communications. In the control system, if the difference between the actual state of the device and the received state does not exceed a required threshold, the user cannot notice the difference. For example, in Tactile Internet, the minimum difference of the force stimulus intensity that our hands can percept is referred to as just noticeable difference (JND) [26]. We define the difference between $\hat{X}_n(k)$ and $X_n(k)$ as $E_n(k) = [e_n^1(k), e_n^2(k), \dots, e_n^F(k)]^T$, where $e_n^j(k) = \hat{x}_n^j(k + D_n^e) - x_n^j(k)$. The JND of this system is denoted as $\Delta = [\delta_1, \delta_2, \dots, \delta_N]^T$. Then, the prediction error probability is given by

$$\varepsilon_n^p = 1 - \prod_{j=1}^N \Pr\{|e_n^j(k)| \leq \delta_j\}, \quad (3)$$

Even if $\hat{X}_n(k)$ is accurate enough, it will be useless if it is not received by the data center before the $(k + D_{\max})$ th slot. Denote the queuing delay bound violation probability and the packet loss probability of the n th device as ε_n^q and ε_n^t , respectively. Then, the overall reliability of the device can be expressed as follows,

$$\varepsilon_n^o = 1 - (1 - \varepsilon_n^q)(1 - \varepsilon_n^t)(1 - \varepsilon_n^p). \quad (4)$$

To achieve ultra-high reliability, all of ε_n^q , ε_n^t and ε_n^p should be small (i.e., less than 10^{-5}). Thus, (4) can be accurately approximated by $\varepsilon_n^o \approx \varepsilon_n^q + \varepsilon_n^t + \varepsilon_n^p$, and the reliability requirement can be satisfied if

$$\varepsilon_n^q + \varepsilon_n^t + \varepsilon_n^p \leq \varepsilon_{\max}. \quad (5)$$

IV. TRADEOFFS IN PREDICTION AND COMMUNICATION SYSTEMS

In this section, we first consider a general linear prediction framework, and derive the relation between the prediction error probability and the prediction horizon in a closed form. Then, we characterize the tradeoff between communication reliability and E2E delay for short packet transmissions in a closed form. Based on the analysis, we further study how to maximize the number of URLLC services that can be supported by the system.

A. State Transition Function

We assume that the state of the n th device, $X_n(k)$, changes according to the following state transition function [27]

$$X_n(k+1) = \Phi_n X_n(k) + W_n(k), \quad (6)$$

where $\Phi_n = [\phi_n^{i,j}]_{F \times F}$, $i, j = 1, 2, \dots, F$, is the state transition matrix and $W_n(k) = [w_n^i(k)]_{F \times 1}$, $i = 1, 2, \dots, F$, is the transition noise. We assume that Φ_n is constant, and thus it can be obtained from measurements or physical laws. The elements of $W_n(k)$ are independent random variables that follow Gaussian distributions with zero mean and variances $\sigma_1^2, \sigma_2^2, \dots, \sigma_F^2$, respectively.

Remark 2. This model is widely adopted in kinematics systems or control systems [27, 28]. Here we consider a general prediction method for a linear system. This is because for non-linear system, the relation between the prediction horizon and the prediction error probability can hardly be derived in a closed-form expression. To implement our framework in non-linear systems, data-driven prediction methods such as neural networks should be applied. These methods do not rely on system models, and will be considered in our future work.

According to (6), the state in the $(k + T_n^p)$ th slot is given by

$$X_n(k + T_n^p) = (\Phi_n)^{T_n^p} X_n(k) + \sum_{i=1}^{T_n^p} (\Phi_n)^{T_n^p - i} W_n(k + i - 1). \quad (7)$$

B. Prediction Horizon and Prediction Error Probability

Inspired by Kalman filter, we consider a general linear prediction method [27]. Based on the system state in the k th slot, we can predict the state in the $(k + 1)$ th slot according to following expression,

$$\hat{X}_n(k + 1) = \Phi_n X_n(k). \quad (8)$$

From (8), we can further predict the state in the $(k + T_n^p)$ th slot,

$$\hat{X}_n(k + T_n^p) = (\Phi_n)^{T_n^p} X_n(k). \quad (9)$$

After T_n^p steps of prediction, the difference between $X_n(k + T_n^p)$ and $\hat{X}_n(k + T_n^p)$ can be derived as follows,

$$\begin{aligned} E_n(k + T_n^p) &\triangleq X_n(k + T_n^p) - \hat{X}_n(k + T_n^p) \\ &= W_n(k + T_n^p - 1) + \sum_{i=1}^{T_n^p-1} (\Phi_n)^{T_n^p-i} W_n(k + i - 1). \end{aligned} \quad (10)$$

The j th element of $E_n(k + T_n^p)$ is given by

$$e_n^j(k + T_n^p) = w_n^j(k + T_n^p - 1) + \sum_{i=1}^{T_n^p-1} \sum_{m=1}^F \phi_{n,j,m,T_n^p-i} w_n^m(k + i - 1), \quad (11)$$

where ϕ_{n,j,m,T_n^p-i} is the element of $(\Phi_n)^{T_n^p-i}$ at the j th row and the m th column.

Since the state transition noises follow independent Gaussian distributions, and $e_n^j(k + T_n^p)$ is a linear combination of them, $e_n^j(k + T_n^p)$ follows a Gaussian distribution with zero mean. The variance of $e_n^j(k + T_n^p)$ is denoted as $\rho_{n,j}^2(T_n^p)$, which is given by

$$\rho_{n,j}^2(T_n^p) = \sigma_j^2 + \sum_{i=1}^{T_n^p-1} \sum_{m=1}^F (\phi_{n,j,m,T_n^p-i})^2 \sigma_m^2. \quad (12)$$

Therefore, $\Pr\{|e_n^j(k + T_n^p)| \leq \delta_j\}$ can be derived as follows,

$$\begin{aligned} \Pr\{|e_n^j(k + T_n^p)| \leq \delta_j\} &= 1 - \Pr\{|e_n^j(k + T_n^p)| > \delta_j\} \\ &= 1 - \psi_{T_n^p,j}(-\delta_j) \\ &= 1 - \psi\left(\frac{-\delta_j}{\rho_{n,j}(T_n^p)}\right), \end{aligned} \quad (13)$$

where $\psi_{T_n^p,j}(\cdot)$ is the cumulative distribution function (CDF) of $e_n^j(k + T_n^p)$, and $\psi(\cdot)$ is the CDF of standard Gaussian distribution with zero mean and unit variance.

By substituting (13) into (3), ε_n^p can be expressed as follows,

$$\varepsilon_n^p = 1 - \prod_{j=1}^F \left[1 - \psi \left(\frac{-\delta_j}{\rho_{n,j}(T_n^p)} \right) \right]. \quad (14)$$

From the expression in (14), we can obtain the following property of ε_n^p .

Lemma 1. ε_n^p strictly increases with the prediction horizon T_n^p .

Proof. Please see Appendix A. □

Lemma 1 indicates that a longer prediction horizon leads to a larger prediction error probability. This is in accordance with the intuition. For example, predicting the mobility of a device in the next 100 ms will be much harder than predicting the mobility in the next 10 ms.

C. Queueing Delay Bound Violation Probability

To derive the queueing delay bound violation probability, ε_n^q , we can use the concept of effective bandwidth [17]. Effective bandwidth is defined as the minimal constant service rate of the queueing system that is required to ensure the maximum queueing delay bound and the delay bound violation probability [29].²

The number of packets generated in each slot depends on the mobility of the device and the random events detected by the device. According to the observation in [31], packet arrival processes in Tactile Internet are very bursty. To capture the burstiness of the packet arrival process, a switched Poisson process (SPP) can be applied [21]³. A SPP includes two traffic states. In each state, the packet arrival process follows a Poisson process. The average packet arrival rates are different in the two states, and the SPP switches between the two states according to a Markov chain. With the traffic state classification methods in [21], the AP knows the average packet arrival rate in the current state, λ_n (packets/slot). According to [17], the effective bandwidth of the Poisson process is given by

$$E_n^B = \frac{\ln(1/\varepsilon_n^q)}{D_n^q \ln \left[\frac{\ln(1/\varepsilon_n^q)}{\lambda_n D_n^q} + 1 \right]} \text{ packets/slot}, \quad (15)$$

²To analyze the upper bound of the delay bound violation probability, a widely used tool is network calculus [30]. However, with network calculus, one can hardly obtain a closed-form expression of the delay bound violation probability. Since we are interested in the asymptotic scenarios that ε_n^q is very small, effective bandwidth can be used [29].

³In standardizations of 3GPP, In standardizations of 3GPP, queueing models are not specified since they depend on specific applications.

which is the minimal constant service rate required to ensure D_n^q and ε_n^q . Since the transmission delay of each packet is fixed as D_n^t , to guarantee the queueing delay violation probability, the following constraint should be satisfied,

$$\frac{1}{D_n^t} = E_n^B. \quad (16)$$

Then, the queueing delay violation probability can be derived as

$$\varepsilon_n^q = e^{D_n^q \phi(\lambda_n, E_n^B)}, \quad (17)$$

where

$$\phi(\lambda_n, E_n^B) = E_n^B \mathbb{W}_{-1} \left(-\frac{\lambda_n}{E_n^B} e^{-\frac{\lambda_n}{E_n^B}} \right) + \lambda_n, \quad (18)$$

where $\mathbb{W}_{-1}(\cdot)$ is the “−1” branch of the Lambert W-function, which is defined as the inverse function of $f(x) = xe^x$. The derivations of (17) and (18) are given in Appendix B.

With the expressions in (17) and (18), we can obtain the following property of ε_n^q .

Lemma 2. ε_n^q strictly decreases with the queueing delay D_n^q when λ_n and E_n^B are given.

Proof. Please see Appendix C. □

Lemma 2 indicates that with the same packet arrival process and service process, the queueing system with a smaller queueing delay bound requirement has a larger queueing delay violation probability. The intuition is that for a given CDF of the steady state queueing delay, the queueing delay violation probability decreases with the queueing delay bound.

D. Packet Loss Probability in Transmissions

With predictions, the communication delay can be longer than the required delay bound D_{\max} (e.g., 1 ms). As such, retransmissions or repetitions becomes possible. To avoid feedback delay caused by retransmissions, we apply K -Repetitions to reduce the packet loss probability in the communication system, i.e., the device sends K copies of each coding block no matter whether the first few copies are successfully decoded or not [6]. The transmission duration of each copy is denoted as D_n^τ . Then, we have $D_n^\tau = D_n^t / K_n$. Some time and frequency resources are reserved for channel estimation at the AP. The fraction of time and frequency resources for data transmission is denoted as $\eta < 1$. To avoid overhead and extra delay caused by channel estimation at the device, we assume the device does not have channel state information (CSI). The impacts of

CSI and training pilots on the achievable rate have been studied in the short blocklength regime [32–35]. If more resource blocks are occupied by pilots, the accuracy of the estimated CSI can be improved. However, the remaining resource blocks for data transmission reduces. How to allocate radio resources for pilots and data transmissions is a complicated problem and deserves further study. By assuming CSI is not available at the transmitters, our approach can serve as a benchmark for future research.

For the transmission of each copy, we assume that the transmission duration is smaller than the channel coherence time and the bandwidth is smaller than the coherence bandwidth. This assumption is reasonable for short packet transmissions in URLLC. Then, the achievable rate in the short blocklength regime over a quasi-static SIMO channel can be accurately approximated by the following normal approximation [15]⁴,

$$b_n \approx \frac{\eta D_n^\tau T_s B_n}{\ln 2} \left[\ln(1 + \gamma_n) - \sqrt{\frac{V_n}{\eta D_n^\tau T_s B_n}} f_Q^{-1}(\varepsilon_n^\tau) \right] \quad (\text{bits/block}), \quad (19)$$

where B_n is the bandwidth, γ_n represents the received SNR, $V_n = 1 - [1 + \gamma_n]^{-2}$ [15], $f_Q^{-1}(\cdot)$ is the inverse function of the Q-function, and ε_n^τ is the decoding error probability. The blocklength of channel codes is $\eta D_n^\tau T_s B_n$. When the blocklength is large, (19) approaches the Shannon capacity⁵.

According to (19), the expected decoding error probability of each transmission over the SIMO channel is given by [15]

$$\bar{\varepsilon}_n^\tau = \int_0^\infty f_Q \left\{ \sqrt{\frac{\eta D_n^\tau T_s B_n}{V_n}} \left[\ln \left(1 + \frac{a_n g_n P_n^t}{\vartheta N_0 B_n} \right) - \frac{b_n \ln 2}{\eta D_n^\tau T_s B_n} \right] \right\} \cdot f_g(x) dx, \quad (20)$$

where $\gamma_n = \frac{a_n g_n P_n^t}{\vartheta N_0 B_n}$ is applied, a_n denotes the large-scale channel gain, g_n is the small-scale channel gain, P_n^t represents the transmit power, $\vartheta > 1$ is the SNR loss due to inaccurate channel estimation, N_0 denotes the noise power spectral density, and $f_g(x)$ is the distribution of the instantaneous channel gain. For Rayleigh fading channel, we have $f_g(x) = \frac{1}{(N_r - 1)!} x^{N_r - 1} e^{-x}$,

⁴The bounds of the decoding error probability can be obtained by using saddlepoint method [36], which is very accurate but has no closed-form expression. Since the gap between the normal approximation and practical coding schemes is around 0.1 dB [37], it is accurate enough for our framework.

⁵The results in [38] indicate that if Shannon capacity is used in the analyses, the delay bound and delay bound violation probability will be underestimated. Thus, the requirements of URLLC cannot be satisfied.

where N_r is the number of antennas at the AP. From the approximation in [39]⁶, $\bar{\varepsilon}_n^\tau$ can be accurately approximated by

$$\bar{\varepsilon}_n^\tau = \frac{\omega_n a_n P_n^t \sqrt{\eta D_n^\tau T_s B_n}}{\vartheta N_0 B_n} \left[(g_n^U - g_n^L) - \sum_{i=0}^{N_r} (N_r - i) A_n^i \right], \quad (21)$$

where $\omega_n = \frac{1}{2\pi\sqrt{2^{2r_n^c}-1}}$, $r_n^c = \frac{b_n}{\eta D_n^\tau T_s B_n}$ is the number bits in each coding block, $g_n^U = \frac{\vartheta N_0 B_n \xi_n}{a_n P_n^t}$, $g_n^L = \frac{\vartheta N_0 B_n \zeta_n}{a_n P_n^t}$, $A_n^i = \frac{(g_n^L)^i}{i!} e^{-g_n^L} - \frac{(g_n^U)^i}{i!} e^{-g_n^U}$, $\xi_n = \theta_n + \frac{1}{2\omega_n \sqrt{\eta D_n^\tau T_s B_n}}$, $\zeta_n = \theta_n - \frac{1}{2\omega_n \sqrt{\eta D_n^\tau T_s B_n}}$, and $\theta_n = 2^{r_n^c - 1}$.

After K repetitions, the packet loss probability in the communication system is given by

$$\varepsilon_n^t = (\bar{\varepsilon}_n^\tau)^{K_n}. \quad (22)$$

From (22), we can obtain the following property of ε_n^t .

Lemma 3. *When D_n^τ is given, ε_n^t strictly decreases with the repetition time K_n .*

Proof. When D_n^τ is given, $\bar{\varepsilon}_n^\tau$ is fixed. According to (22), ε_n^t decreases with K_n since $\bar{\varepsilon}_n^\tau < 1$. \square

Lemma 3 indicates that there is a tradeoff between the transmission delay and the reliability in communications. K -Repetition can be used to improve the transmission reliability at the cost of increasing the transmission delay.

V. PREDICTION AND COMMUNICATION CO-DESIGN

In the above tradeoff analyses, we obtained closed-form relations between each delay component (or prediction horizon) and its corresponding packet loss factor in terms of prediction, queueing and wireless transmission, respectively. Based on the above analyses, the tradeoff between the overall reliability and prediction horizon is revealed. As such, we could formulate the optimization problem in the following subsection.

A. Problem Formulation

To maximize the number of devices that can be supported by the system, we optimize the delay components, prediction horizon, and bandwidth allocation of wireless networks. The optimization problem can be formulated as follows,

⁶As validated in [39], the approximation in (21) is accurate, especially when the number of antennas is large or the packet loss probability is small.

$$\max_{\substack{D_n^q, D_n^t, T_n^p, B_n, \\ n=1, \dots, N}} N \quad (23)$$

$$\text{s.t.} \quad \sum_{n=1}^N B_n \leq B_{\max}, \quad (23a)$$

$$D_n^q + D_n^t + D_n^d + D_n^r - T_n^p \leq D_{\max}, \quad (23b)$$

$$\varepsilon_n^q + \varepsilon_n^t + \varepsilon_n^p \leq \varepsilon_{\max}, \quad (23c)$$

$$\varepsilon_n^q = \exp \left\{ D_n^q \left[\frac{\mathbb{W}_{-1}(-\lambda_n D_n^t e^{-\lambda_n D_n^t})}{D_n^t} + \lambda_n \right] \right\}, \quad (23d)$$

$$\varepsilon_n^t = \left\{ \frac{\omega_n a_n P_n^t \sqrt{\eta D_n^r T_s B_n}}{\vartheta N_0 B_n} \left[(g_n^U - g_n^L) - \sum_{i=0}^{N_r} (N_r - i) A_n^i \right] \right\}^{K_n}, \quad K_n D_n^r = D_n^t \quad (23e)$$

$$\varepsilon_n^p = 1 - \prod_{j=1}^F \left[1 - \psi \left(\frac{-\delta_j}{\sqrt{\sigma_j^2 + \sum_{i=1}^{T_n^p-1} \sum_{m=1}^F (\phi_{n,j,m,T_n^p-i})^2 \sigma_m^2}} \right) \right], \quad (23f)$$

$$n = 1, 2, 3, \dots, N, \quad (23g)$$

where (23a) is the constraint on total bandwidth, (23b) is the constraint on user experienced delay, (23c) is the constraint on reliability. (23d) is obtained by substituting (18) and (16) into (17), (23e) is obtained from (21) and (22), and (23f) is obtained by substituting (12) into (14).

Problem (23) is not a deterministic optimization problem since the numbers of optimization variables and constraints depend on the number of users, which is not given. In addition, some optimization variables are integers and the constraints in (23c), (23d), and (23e) are non-convex. Thus, it is very challenging to solve this problem.

B. Algorithm for Solving Problem (23)

To solve the problem (23), we first find the minimal bandwidth B_n required for each user to ensure its delay and reliability requirements, i.e., $(D_{\max}, \varepsilon_{\max})$. By minimizing the bandwidth allocated to each user, the total number of users that can be supported with a given amount of

total bandwidth can be maximized. Without the constraint on total bandwidth, the problem (23) can be decomposed into multiple single-user problems:

$$\min_{D_n^q, D_n^t, T_n^p} B_n \quad (24)$$

$$\text{s.t. (23b), (23c), (23d), (23e) and (23f).} \quad (25)$$

To solve the above problem, we need the minimal bandwidth that is required to ensure a certain overall reliability. We denote it as $B_n^{\min}(\varepsilon_n^o)$. However, deriving the expression of $B_n^{\min}(\varepsilon_n^o)$ is very difficult. To overcome this difficulty, we first minimize ε_n^o for a given B_n . Then, we find the minimal required bandwidth that can satisfy $\varepsilon_n^o \leq \varepsilon_{\max}$ via binary search.

When B_n is given, the minimal overall error probability can be obtained by optimizing T_n^p in solving the following problem,

$$\varepsilon_n^{o,\min}(B_n) = \min_{D_n^q, D_n^t, T_n^p} \varepsilon_n^q + \varepsilon_n^t + \varepsilon_n^p \quad (26)$$

$$\text{s.t. (23b), (23d), (23e) and (23f),}$$

For mathematical tractability, we set $\varepsilon_n^q = \varepsilon_n^t$. According to [17], this simplification leads to negligible performance loss. We will first prove ε_n^q and ε_n^t decreases with T_n^p in the Proposition 1 when $\varepsilon_n^q = \varepsilon_n^t$.

Proposition 1. ε_n^q and ε_n^t decrease with T_n^p when $\varepsilon_n^q = \varepsilon_n^t$.

Proof. Please see Appendix D. □

Proposition 1 reveals the relation between the reliability of the queueing system (or the reliability of the wireless link) and the prediction horizon. With this relation, the number of independent optimization variables can be reduced.

It can be recalled that ε_n^p increases with T_n^p . Thus, together with Proposition 1, the optimal solution is obtained when the equality in (27) holds, which is

$$D_n^q + D_n^t + D_n^r - T_n^p = D_{\max}. \quad (27)$$

Moreover, for a given value of T_n^p , the values of D_n^q and D_n^t that satisfies $\varepsilon_n^q = \varepsilon_n^t$ and (27) can be obtained via binary search. Therefore, we only need to optimize T_n^p in problem (26). The

optimal solution and the minimal overall reliability in this simplified scenario are denoted as T_n^{p*} and $\varepsilon_n^{\text{o,min*}}(B_n)$, respectively.

Unfortunately, the simplified problem is still non-convex. As such, we will propose an approximated solution as follows. According to Lemma 1, ε_n^p increases with T_n^p , and we have proved ε_n^q and ε_n^t decreases with T_n^p in Proposition 1. A near optimal solution can be obtained when $\varepsilon_n^q + \varepsilon_n^t = \varepsilon_n^p$. Since the optimization variables are not integers, $\varepsilon_n^q + \varepsilon_n^t = \varepsilon_n^p$ may not hold strictly. To address this issue, we can use binary search to find \tilde{T}_n^p that satisfies $\varepsilon_n^p \leq 2\varepsilon_n^t$ when $T_n^p \leq \tilde{T}_n^p$, and $\varepsilon_n^p > 2\varepsilon_n^t$ when $T_n^p > \tilde{T}_n^p$. The corresponding reliability is denoted as $\hat{\varepsilon}_n^{\text{o,min}}(B_n)$. The overall reliability achieved by this near optimal solution is denoted as $\hat{\varepsilon}_n^{\text{o,min}}(B_n)$.

The performance gap between the near optimal solution and optimal one is analyzed in the following Proposition 2.

Proposition 2. *The gap between $\hat{\varepsilon}_n^{\text{o,min}}(B_n)$ and $\varepsilon_n^{\text{o,min*}}(B_n)$ is less than $\varepsilon_n^{\text{o,min*}}(B_n)$, where $\varepsilon_n^{\text{o,min*}}(B_n)$ is the reliability achieved by the optimal solution.*

Proof. Please see Appendix E. □

Proposition 2 shows that the gap between the near optimal overall reliability and the optimal one is bounded by the value of the optimal overall reliability. Since the optimal overall reliability is in the order of 10^{-5} , the gap is very small.

The required minimal bandwidth to guarantee the overall reliability can be obtained from the following optimization problem,

$$\min_{B_n} B_n \tag{28}$$

$$\text{s.t. } \hat{\varepsilon}_n^{\text{o,min}}(B_n) \leq \varepsilon_{\max}. \tag{28a}$$

Since the packet loss in the communication system decreases with bandwidth, the optimal solution of problem (28) is achieved when the equality in (28a) holds. Thus, the minimal bandwidth can be obtained via binary search. The algorithm to solve problem (24) is summarized in Table II.

C. Discussions on Implementation Complexity and Optimality

The original optimization problem is decomposed into N single-user problems. To solve each single-user problem, we search the required bandwidth and optimal prediction horizon in

the regions $[0, \bar{B}]$ and $[0, \bar{T}^p]$, respectively, where \bar{B} and \bar{T}^p are the upper bounds of bandwidth and prediction horizon. Therefore, the complexity of the proposed algorithm is around $\mathcal{O}(N \log_2(\bar{B}) \log_2(\bar{T}^p))$.

The performance loss of the near optimal solution relative to the global optimal solution results from simplification $\varepsilon_n^q = \varepsilon_n^t$ and the differences between $\hat{\varepsilon}_n^{o,\min}(B_n)$ and $\varepsilon_n^{o,\min^*}(B_n)$. According to the analysis in [17] and Proposition 2, the performance loss is minor. We will further validate the performance loss with numerical results.

TABLE II
ALGORITHM TO SOLVE (24)

Input: User-experienced delay requirement D_{\max} , reliability requirement ε_{\max} , user number N , average packet arrival rate λ_n , each packet duration D^τ , slot duration T_s , bandwidth of each subcarrier B_0 , upper bound of bandwidth \bar{B} , upper bound of prediction horizon \bar{T}^p , transmit power P^t , user location d_n transition noise σ_j , initial noise σ_j , threshold δ_j , $j = 1, 2, \dots, F$.

Output: The minimal bandwidth B_n^* to ensure URLLC for the n th user.

- 1: $B_L = B_0, B_R = \bar{B}$.
- 2: $B_b = \frac{1}{2}(B_L + B_R)$.
- 3: Binary search T_n^p in a range of $(0, \bar{T}^p]$ and obtain $\hat{\varepsilon}_n^{o,\min}(B_b)$.
- 4: **while** $|\hat{\varepsilon}_n^{o,\min}(B_b) - \varepsilon_{\max}| < \varepsilon_{\max}$ **do**
- 5: **if** $\hat{\varepsilon}_n^{o,\min}(B_b) > \varepsilon_{\max}$ **then**
- 6: $B_L = B_b$.
- 7: **else**
- 8: $B_R = B_b$.
- 9: **end if**
- 10: $B_b = \frac{1}{2}(B_L + B_R)$.
- 11: Binary search T_n^p in a range of $(0, \bar{T}^p]$ and obtain $\hat{\varepsilon}_n^{o,\min}(B_b)$.
- 12: **end while**
- 13: **return** $B_n^* = B_b$.

VI. PERFORMANCE EVALUATION

In this section, we evaluate the effectiveness of the proposed co-design method via simulations and experiments.

A. Simulations

In the simulations, we consider a one-dimensional movement as an example to evaluate the proposed co-design method. With this example, we show how the proposed method helps improving the tradeoffs among latency, reliability and resource utilizations (i.e., bandwidth and antenna). For comparison, the performance achieved by the traditional transmission scheme with

no prediction is provided. The simulation parameters are listed in Table III. In all simulations, SNRs are computed according to $\gamma_n = \frac{a_n g_n P_n^t}{\vartheta N_0 B_n}$. The path loss model is $10 \log_{10}(a_n) = 35.3 + 37.6 \log_{10}(d_n) + S_n$, where d_n is the distance from the n th device to the AP and S_n is the shadowing. The shadowing S_n follows log normal distribution with a zero mean and a standard deviation of 8. To ensure the reliability and latency requirements, we consider the worst case of shadowing $S_w = -34.1$ dB (i.e., $\Pr\{S_n \leq S_w\} = 10^{-5}$), which is defined as the probability that the delay and reliability of a device can be satisfied [39].

For the one-dimensional movement, the state transition function in (6) can be simplified as follows [27],

$$\begin{bmatrix} r(k+1) \\ v(k+1) \\ a(k+1) \end{bmatrix} = \begin{bmatrix} 1 & T_s & \frac{T_s^2}{2} \\ 0 & 1 & T_s \\ 0 & 0 & 1 \end{bmatrix} \begin{bmatrix} r(k) \\ v(k) \\ a(k) \end{bmatrix} + \begin{bmatrix} 0 \\ 0 \\ w(k) \end{bmatrix}.$$

where $r(k)$, $v(k)$, and $a(k)$ represent the location, velocity and acceleration in the k th slot, respectively, $w(k)$ is the Gaussian noise on acceleration, and Φ is given by

$$\Phi = \begin{bmatrix} 1 & T_s & \frac{T_s^2}{2} \\ 0 & 1 & T_s \\ 0 & 0 & 1 \end{bmatrix}, \quad (29)$$

which follows Newton's laws of motion. In predictions, the standard deviation of the transition noise of acceleration is $\sigma_w = 0.01$ m/s², and the required threshold is $\delta_l = 0.1$ m. The standard derivatives of the initial errors of location, velocity and acceleration are set to be 0.01 m, 0.2 m/s, and 0.1 m/s², respectively. In practice, the values of initial errors depend on the accuracy of observation and residual filter errors [27].

1) *Single-user scenarios*: In single-user scenarios, the distance between the user and the AP is set to be 200 m. To evaluate the proposed co-design method, the prediction horizon T_n^p is optimized to obtain the minimal overall error probability.

Under the given delay requirement (i.e., $D_{\max} = 0$ ms), the packet loss probability in communications ε_n^c , the prediction error probability ε_n^p , and the overall error probability ε_n^o are shown in Fig. 3. To achieve target reliability, the bandwidth B is set as $B = 440$ KHz and the number of antennas at the AP is set to be $N_r = 32$. It should be noted that the reliability depends on the amount of bandwidth and the number of antennas, but the trend of the overall reliability does not change.

TABLE III
SIMULATION PARAMETERS [2]

Parameters	Values
Maximal transmit power of a user P_t	23 dBm
Single-sided noise spectral density N_0	-174 dBm/Hz
Information load per block b	160 bits
Average packet arrival rate λ	100 packets/second
Slot duration T_s	0.1 ms
Transmission duration D_τ	0.5 ms
Delay of core network and backhaul D_r	10 ms

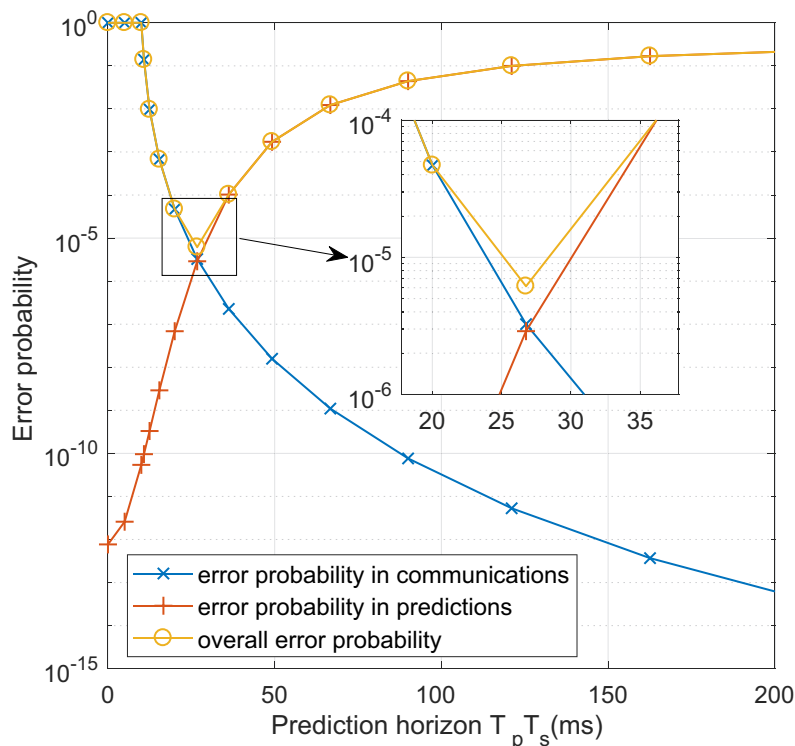


Fig. 3. Joint optimization of predictions and communications: the packet loss probability ε_c in communications, the prediction error probability ε_p , and the over error probability ε_o are drawn as functions of prediction horizon $T_p T_s$.

In Fig. 3, the communication delay and prediction horizon are set to be equal, i.e., $D_n^q + D_n^t = T_n^p$. In this case, user experienced delay is zero. The results in Fig. 3 show that when the E2E communication delay $D_n^q + D_n^t = T_n^p < 10$ ms, i.e., less than the delays in the core network and the backhaul D_r , it is impossible to achieve zero latency without prediction. When $D_n^q + D_n^t = T_n^p > 10$ ms, the required transmission duration $K D_n^r$ increases with prediction horizon T_n^p . As a result, the overall error probability, ε_n^o , is first dominated by ε_n^c and then by

ε_n^p . As such, ε_n^o first decreases and then increases with T_n^p . The results in Fig. 3 indicate that the reliability achieved by the proposed method is 6.52×10^{-6} with $T_n^p = 26.8$ ms, $D_n^{t*} = 12.5$ ms, $D_n^{q*} = 14.3$ ms and $K_n^* = 5$. The optimal solution obtained by exhaustive search is 6.15×10^{-6} . The gap between above two solutions is 3.7×10^{-7} , which is very small.

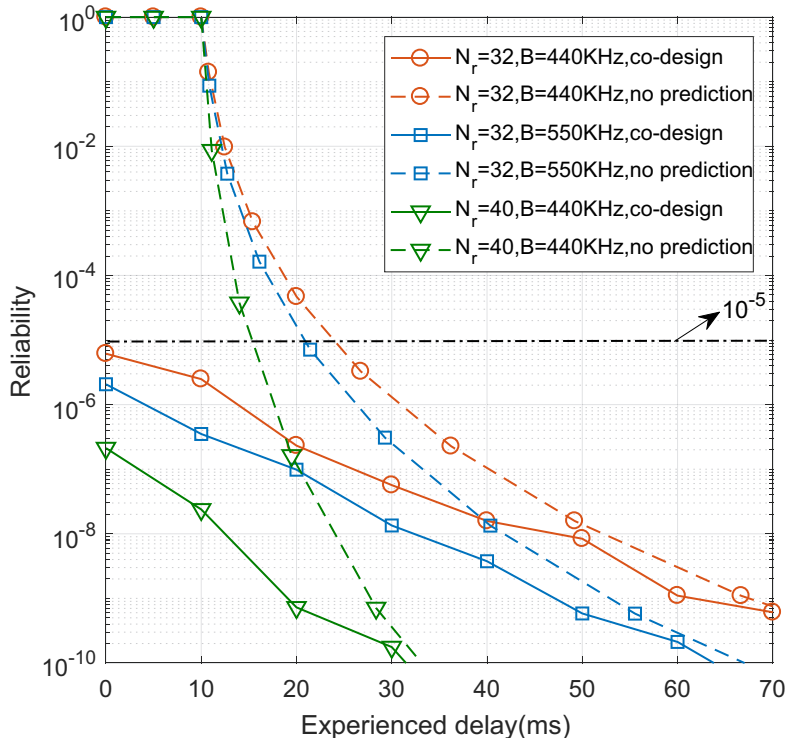


Fig. 4. Comparison of reliability-delay tradeoff curves between co-design and no predictions with different bandwidth B and numbers of received antennas N_r .

In Fig. 4, the proposed co-design method is compared with a baseline method without prediction. When there is no prediction, the user experienced delay equals to communication delay. The results in Fig. 4 show that when the requirement on user experienced delay is less than 10 ms, it cannot be satisfied without prediction. When the required user experienced delay is larger than 10 ms, the reliability achieved by the co-design method is much better than the baseline method. In other words, by prediction and communication co-design, the tradeoff between user experienced delay and overall reliability can be improved remarkably. Particularly, in the case $N_r = 32$ and $B = 440$ KHz, to ensure the same reliability 10^{-5} , the user experienced delay can be reduced by 23 ms and zero-latency can be achieved by the proposed co-design method.

2) *Multiple-user scenarios*: In multiple-user scenarios, we will consider two scenarios: the

distribution of large-scale fading of the mobile devices is available/unavailable. In the first scenario, the distances from devices to the AP are uniformly distributed in the region $[50, 200]$ m. In the second scenario, the worst case is considered in the optimization, i.e., the distances from all the devices to the AP are 200 m.

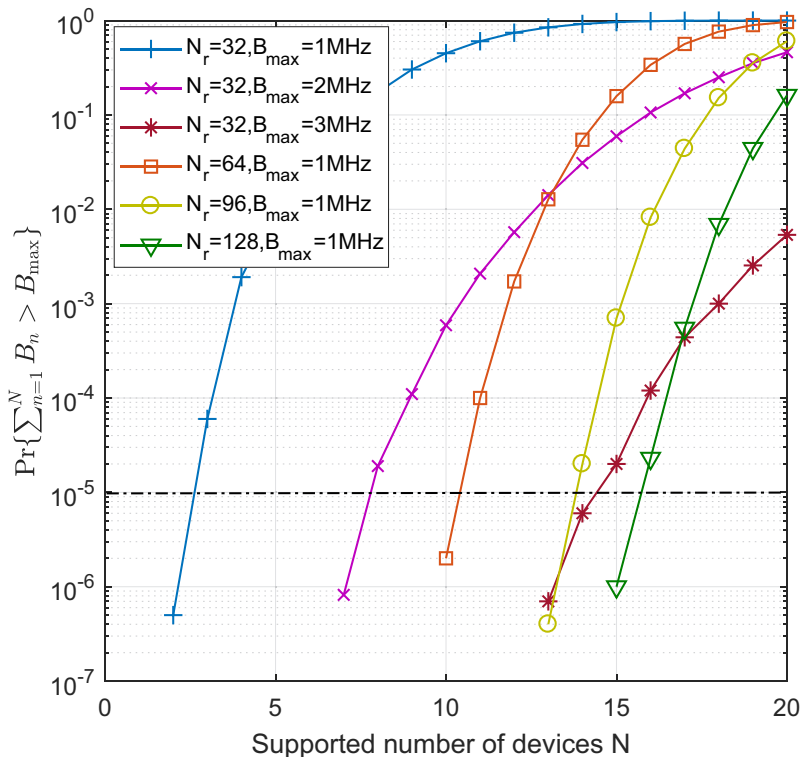


Fig. 5. $\Pr\{\sum_{n=1}^N B_n > B_{\max}\}$ v.s. the number of devices when the distribution of large-scale fading of devices is known.

Since the large-scale fading of devices are random variables in the first scenario, the sum of the required bandwidth is also a random variable. In Fig. 5, we illustrated the probability that the sum of the required bandwidth is smaller than B_{\max} . For URLLC services, we need to guarantee the delay and reliability requirements with high probability, e.g., 99.999 %. The results in Fig. 5 show that when $B_{\max} = 1$ MHz and $N_r = 32$, the system can only support 2 devices. By doubling the number of antennas (or the total bandwidth), 10 (or 7) devices can be supported. This implies that increasing the number of antennas at the AP is an efficient way to increase the number of devices that can be supported by the system. This is because SNR increases with the number of antennas due to array gain. To achieve the same reliability, i.e., packet loss probability, higher order modulation schemes can be used if more antennas are deployed at the AP. Since the

spectrum efficiency increases with the order of the modulation scheme, more URLLC devices can be supported with a given amount of bandwidth.

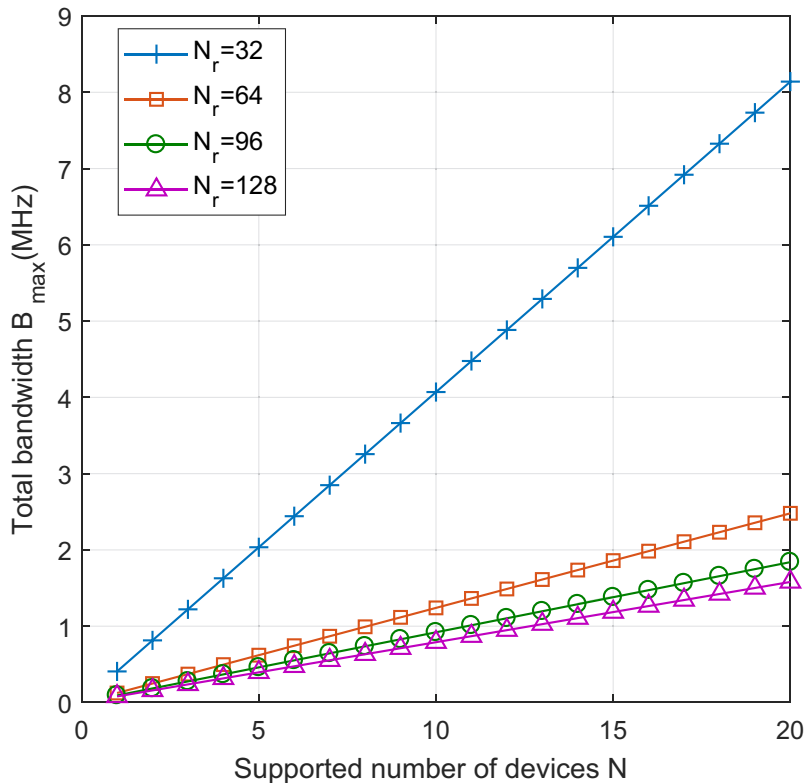


Fig. 6. Required total bandwidth v.s. number of devices when the distribution of large-scale fading of devices is unknown.

If the distribution of large-scale fading of devices is unknown, the worst case is considered. Then, the total bandwidth that is required to support a given number of devices is deterministic. The results in Fig. 6 show that the required total bandwidth linearly increases with the number of devices. This is because the required bandwidth for different devices are the same since the worst case is considered for all the devices. In addition, by increasing the number of antennas from 32 to 64, we can save 75 % of bandwidth. This implies that increasing the number of antennas is an efficient way to improve spectrum efficiency of URLLC.

B. Experiments

To validate whether mobility prediction works for URLLC in practice, we record the real movement data from the experiment shown in Fig. 7. In this experiment, a typical application of Tactile Internet is implemented in a virtual environment, where a box of hazardous chemicals

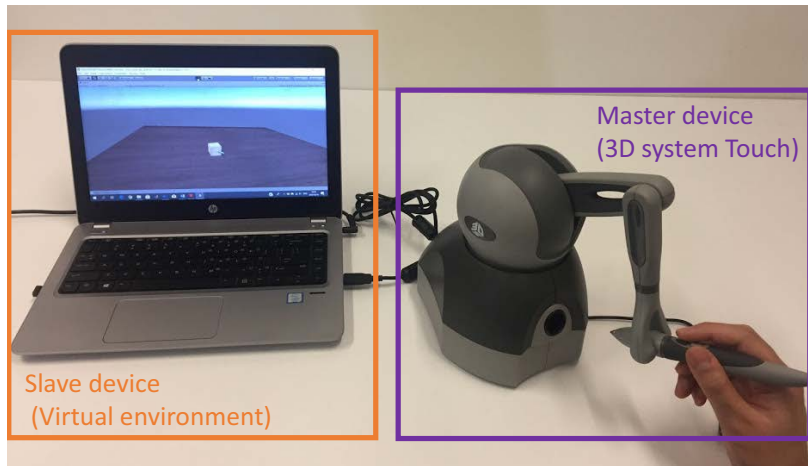


Fig. 7. Experiment to obtain real movement data in Tactile Internet.

or radioactive substances is dragged to move on the floor by a virtual slave device. A tactile hardware device named 3D System Touch (previously named Phantom Omni, or Geomagic) is used as a master device, which sends real time location information to the virtual slave device. A cable is used to connect the master device to the virtual slave device in a virtual environment. The slave device in the virtual environment receives the locations from the master device, so it can move synchronously with the master device.

Human operators are invited to drag the virtual box from one corner to another corner of the floor in the virtual environment. In this experiment, we mainly interested in the motion prediction, so the location information on the x-axis produced by the tactile hardware device is recorded and used to verify the predictions. A general linear prediction method in (9) is used to predict the future state system. Since only location information is available from the hardware, the velocity and acceleration are obtained from the first and the second order differences of locations [40]. Moreover, due to the limitation of the hardware, the duration of each slot is $T_s = 1$ ms.

The prediction error probabilities, ε_n^p , with different thresholds, δ , are shown in Table IV, where the prediction horizon, nT_s , is fixed. The results in Table IV show that for the constant prediction horizon $nT_s = 5$ ms or $nT_s = 20$ ms, ε_n^p decreases with the required threshold δ .

The relation between the prediction error probability and the prediction horizon is shown in Table V, where the required threshold is fixed. The results indicate that ε_n^p increases with nT_s . This observation consists with Lemma 1.

TABLE IV
PREDICTION ERROR PROBABILITY WITH FIXED nT_s

$\delta(m)$	$\varepsilon_n^p (nT_s = 5 \text{ ms})$	$\varepsilon_n^p (nT_s = 20 \text{ ms})$
0.002	2.95×10^{-4}	0.45
0.01	1.62×10^{-5}	0.42
0.02	6.61×10^{-6}	3.2×10^{-3}
0.1	2.40×10^{-6}	2.40×10^{-5}
0.2	1.80×10^{-6}	7.82×10^{-6}

TABLE V
PREDICTION ERROR PROBABILITY WITH GIVEN δ

$nT_s(\text{ms})$	$\varepsilon_n^p (\delta = 0.002 \text{ m})$	$nT_s(\text{ms})$	$\varepsilon_n^p (\delta = 0.2 \text{ m})$
1	3.00×10^{-6}	10	1.80×10^{-6}
2	1.62×10^{-5}	20	7.82×10^{-6}
3	3.49×10^{-5}	30	2.71×10^{-5}
4	5.77×10^{-5}	40	4.45×10^{-5}
5	2.95×10^{-4}	50	1.69×10^{-4}

The results in Tables IV and V imply that prediction and communication co-design has the potential to achieve zero-latency in practice. It should be noted that the results from the experiment are generally worse than those of the simulations. This is because we only have the location information of the device, and extra estimation errors are introduced during the estimations of the velocity and acceleration.

VII. CONCLUSIONS

In this paper, we studied how to achieve URLLC by prediction and communication co-design. We first derived the decoding error probability, the queueing delay violation probability, and the prediction error probability in closed-form expressions. Then, we established an optimization framework for maximizing the number of devices that can be supported in a system by optimizing time and frequency resources in the communication system and the prediction horizon in the prediction system. Simulation results show that by prediction and communication co-design the tradeoff between delay and reliability can be improved remarkably, or we can improve the spectrum efficiency subject to the delay and reliability constraints. In addition, an experiment was carried out to validate the accuracy of prediction in a remote-control system. The results

showed that the proposed concept on prediction and communication co-design works well in the practical remote-control system.

APPENDIX A

PROOF OF LEMMA 1

Proof. To prove this lemma, we need to prove that for any $T_n^{p,1} < T_n^{p,2}$, $\varepsilon_n^p(T_n^{p,1}) < \varepsilon_n^p(T_n^{p,2})$ holds. From (12), we have

$$\sigma_j^2(T_n^p + 1) - \sigma_j^2(T_n^p) = \sum_{m=1}^F \phi_{n,j,m,n} \sigma_m^2 > 0.$$

As such, we can conclude that $\sigma_j(T_n^p)$, $j = 1, 2, \dots, N$, increases with T_n^p .

Moreover, from (14), we can see that ε_n^p increases with $\sigma_j(T_n^p)$, $j = 1, 2, \dots, N$. Therefore, ε_n^p increases with the prediction horizon T_n^p . This completes the proof. \square

APPENDIX B

DERIVATIONS OF (17) AND (18)

The equation (15) can be re-expressed as

$$\frac{\ln(1/\varepsilon_n^q) + \lambda_n D_n^q}{\lambda_n D_n^q} = \exp \left[\frac{\ln(1/\varepsilon_n^q) + \lambda_n D_n^q}{D_n^q E_n^B} - \frac{\lambda_n}{E_n^B} \right], \quad (30)$$

and

$$-\frac{\lambda_n}{E_n^B} \exp \left(-\frac{\lambda_n}{E_n^B} \right) = \frac{\ln(1/\varepsilon_n^q) + \lambda_n D_n^q}{-D_n^q E_n^B} \exp \left[\frac{\ln(1/\varepsilon_n^q) + \lambda_n D_n^q}{-D_n^q E_n^B} \right]. \quad (31)$$

According to the definition of Lambert function, (31) can be written as

$$\frac{\ln(1/\varepsilon_n^q) + \lambda_n D_n^q}{-D_n^q E_n^B} = \mathbb{W} \left[-\frac{\lambda_n}{E_n^B} \exp \left(-\frac{\lambda_n}{E_n^B} \right) \right]. \quad (32)$$

It should be noted that when $-\frac{\lambda_n}{E_n^B} \exp \left(-\frac{\lambda_n}{E_n^B} \right) < 0$, the Lambert function has two branches according to the range of $\frac{\ln(1/\varepsilon_n^q) + \lambda_n D_n^q}{D_n^q E_n^B}$. Specifically, we have

$$\frac{\ln(1/\varepsilon_n^q) + \lambda_n D_n^q}{-D_n^q E_n^B} = \begin{cases} \mathbb{W}_0 \left[-\frac{\lambda_n}{E_n^B} \exp \left(-\frac{\lambda_n}{E_n^B} \right) \right], & -1 < \frac{\ln(1/\varepsilon_n^q) + \lambda_n D_n^q}{-D_n^q E_n^B} < 0 \\ \mathbb{W}_{-1} \left[-\frac{\lambda_n}{E_n^B} \exp \left(-\frac{\lambda_n}{E_n^B} \right) \right], & \frac{\ln(1/\varepsilon_n^q) + \lambda_n D_n^q}{-D_n^q E_n^B} \geq 0 \end{cases} \quad (33)$$

In the first case in (33), $\mathbb{W}_0 \left[-\frac{\lambda_n}{E_n^B} \exp \left(-\frac{\lambda_n}{E_n^B} \right) \right] = -\frac{\lambda_n}{E_n^B} = \frac{\ln(1/\varepsilon_n^q) + \lambda_n D_n^q}{-D_n^q E_n^B}$. We can obtain that $\varepsilon_n^q = 1$, which does not satisfy the reliability requirement. Thus, the first case in (33) can be removed. As such, we have

$$\frac{\ln(1/\varepsilon_n^q) + \lambda_n D_n^q}{-D_n^q E_n^B} = \mathbb{W}_{-1} \left[-\frac{\lambda_n}{E_n^B} \exp \left(-\frac{\lambda_n}{E_n^B} \right) \right], \quad (34)$$

and

$$\varepsilon_n^q = \exp \left\{ D_n^q E_n^B \mathbb{W}_{-1} \left[-\frac{\lambda_n}{E_n^B} \exp \left(-\frac{\lambda_n}{E_n^B} \right) \right] + D_n^q \lambda_n \right\}. \quad (35)$$

APPENDIX C

PROOF OF LEMMA 2

Proof. According to (17), we have

$$\ln(\varepsilon_n^q) = D_n^q \phi(\lambda_n, E_n^B). \quad (36)$$

Since ε_n^q is in the order of 10^{-5} to 10^{-8} and $D_n^q > 0$, $\ln(\varepsilon_n^q) < 0$, and thus $\phi(\lambda_n, E_n^B) < 0$. As such, ε_n^q decreases with D_n^q in (17) when $\phi(\lambda_n, E_n^B)$ is given. The proof follows. \square

APPENDIX D

PROOF OF PROPOSITION 1

Proof. According to (27), we have $D_n^q + D_n^t = D_{\max} + T_n^p - D_n^r$. To prove this proposition, we need to prove that ε_n^q or ε_n^t decreases with $D_n^q + D_n^t$.

Next, we will prove D_n^q increases with D_n^t , and thus $D_n^q + D_n^t$ increases with D_n^t . According to (17) and (18), we have

$$D_n^q = \frac{\ln(\varepsilon_n^q)}{\phi(\lambda_n, E_n^B)},$$

where

$$\phi(\lambda_n, E_n^B) = \frac{\mathbb{W}_{-1}(-\lambda_n D_n^t e^{-\lambda_n D_n^t})}{D_n^t} + \lambda_n.$$

To check the monotonicity of D_n^q in terms of ε_n^q and D_n^t , we have the following partial derivatives,

$$\frac{\partial D_n^q}{\partial \varepsilon_n^q} = \frac{1}{\varepsilon_n^q \phi(\lambda_n, E_n^B)} < 0, \quad (37)$$

and

$$\frac{\partial D_n^q}{\partial D_n^t} = \frac{\ln(\varepsilon_n^q) \mathbb{W}_{-1}(-\lambda_n D_n^t e^{-\lambda_n D_n^t})}{[\mathbb{W}_{-1}(-\lambda_n D_n^t e^{-\lambda_n D_n^t}) + 1] [\mathbb{W}_{-1}(-\lambda_n D_n^t e^{-\lambda_n D_n^t}) + \lambda_n D_n^t]} > 0. \quad (38)$$

As such, we prove D_n^q increases with D_n^t when ε_n^q is given. According to Lemma 3, ε_n^t strictly decreases with the transmission delay D_n^t . Since $\varepsilon_n^q = \varepsilon_n^t$, ε_n^q also strictly decreases with the transmission delay D_n^t . According to (37), D_n^q increases with a smaller ε_n^q . So D_n^q increases with D_n^t when ε_n^q is determined by D_n^t .

In summary, ε_n^q or ε_n^t decreases with D_n^t and $D_n^q + D_n^t$, and thus decreases with T_n^p . This completes the proof. □

APPENDIX E

PROOF OF PROPOSITION 2

Proof. In this appendix, we use the notation $\varepsilon_n^o(T_n^p, B_n)$, (or $\varepsilon_n^t(T_n^p, B_n)$ or $\varepsilon_n^p(T_n^p, B_n)$) to represent the relationship between the prediction horizon and the overall reliability (or the decoding error probability or the prediction error probability). For notational simplicity, we first omit B_n .

To prove this proposition, we first introduce an upper bound of $\varepsilon_n^o(T_n^p) = 2\varepsilon_n^t(T_n^p + D_{\max}) + \varepsilon_n^p(T_n^p)$, i.e., $\varepsilon_n^{\text{ub}}(T_n^p) = 2 \max\{2\varepsilon_n^t(T_n^p + D_{\max}), \varepsilon_n^p(T_n^p)\}$.

Suppose \tilde{T}_n^p is the maximal prediction horizon that satisfies $2\varepsilon_n^t(T_n^p + D_{\max}) - \varepsilon_n^p(T_n^p) > 0$ for all $0 \leq T_n^p \leq \tilde{T}_n^p$, and hence $\varepsilon_n^{\text{ub}}(T_n^p) = 4\varepsilon_n^t(T_n^p + D_{\max})$, which strictly decreases with T_n^p . On the other hand, when $T_n^p > \tilde{T}_n^p$, $2\varepsilon_n^t(T_n^p + D_{\max}) - \varepsilon_n^p(T_n^p) < 0$, and hence $\varepsilon_n^{\text{ub}}(T_n^p) = 2\varepsilon_n^p(T_n^p)$, which strictly increases with T_n^p . In other words, $\varepsilon_n^{\text{ub}}(T_n^p)$ strictly decreases with T_n^p when $T_n^p \leq \tilde{T}_n^p$ and strictly increases with T_n^p when $T_n^p > \tilde{T}_n^p$. Therefore, the upper bound $\varepsilon_n^{\text{ub}}(T_n^p)$ is minimized at $\hat{T}_n^p = \tilde{T}_n^p$ or $\hat{T}_n^p = \tilde{T}_n^p + 1$.

Let $2\varepsilon_n^t(\hat{T}_n^p + D_{\max}) - \varepsilon_n^p(\hat{T}_n^p) = \Delta$, where Δ is the small gap between $2\varepsilon_n^t$ and ε_n^p at \hat{T}_n^p , which is every closed to zero. We have

$$\varepsilon_n^o(\hat{T}_n^p) \approx \varepsilon_n^{\text{ub}}(\hat{T}_n^p), \quad (39)$$

Besides, $\varepsilon_n^{\text{ub}}(\hat{T}_n^p)$ is the minimum of $\varepsilon_n^{\text{ub}}(T_n^p)$, $\forall n \in [0, \infty)$, and hence

$$\varepsilon_n^{\text{ub}}(\hat{T}_n^p) \leq \varepsilon_n^{\text{ub}}(T_n^{p*}), \quad (40)$$

where T_n^{p*} is the optimal prediction horizon that minimizes $\varepsilon_n^o(T_n^p)$. According to the definition

of $\varepsilon_n^{\text{o,ub}}(T_n^p)$, we have

$$\begin{aligned}
\varepsilon_n^{\text{o,ub}}(T_n^{p*}) &= 2 \max\{2\varepsilon_n^{\text{t}}(T_n^{p*} + D_{\max}), \varepsilon_n^{\text{p}}(T_n^{p*})\} \\
&< 2 [2\varepsilon_n^{\text{t}}(T_n^{p*} + D_{\max}) + \varepsilon_n^{\text{p}}(T_n^{p*})] \\
&= 2\varepsilon_n^{\text{o}}(T_n^{p*}).
\end{aligned} \tag{41}$$

From (39), (40) and (41), we have $\varepsilon_n^{\text{o}}(\hat{T}_n^p) < 2\varepsilon_n^{\text{o}}(T_n^{p*})$, i.e., $\varepsilon_n^{\text{o}}(\hat{T}_n^p) - \varepsilon_n^{\text{o}}(T_n^{p*}) < \varepsilon_n^{\text{o}}(T_n^{p*})$.

Since $\varepsilon_n^{\text{o}}(\hat{T}_n^p)$ and $\varepsilon_n^{\text{o}}(T_n^{p*})$ are defined as $\hat{\varepsilon}_n^{\text{o,min}}(\hat{T}_n^p, B_n)$ and $\varepsilon_{\text{o,n}}^{\text{min}*}(T_n^{p*}, B_n)$, respectively. So we have $\hat{\varepsilon}_n^{\text{o,min}}(\hat{T}_n^p, B_n) - \varepsilon_{\text{o,n}}^{\text{o,min}*}(T_n^{p*}, B_n) < \varepsilon_{\text{o,n}}^{\text{o,min}*}(T_n^{p*}, B_n)$. The proof follows. \square

REFERENCES

- [1] Z. Hou, C. She, Y. Li, and B. Vucetic, "Ultra-reliable and low-latency communications: prediction and communication co-design," in *Proc. IEEE ICC*, 2019.
- [2] 3GPP TSG RAN TR38.913 R14, "Study on scenarios and requirements for next generation access technologies," Jun. 2017.
- [3] L. Kang, W. Zhao, B. Qi, and S. Banerjee, "Augmenting self-driving with remote control: Challenges and directions," in *Proc. ACM Mobile Computing Systems & Applications*, 2018, pp. 19–24.
- [4] G. Zhao, M. A. Imran, Z. Pang, Z. Chen, and L. Li, "Toward real-time control in future wireless networks: communication-control co-design," *IEEE Commun. Mag.*, vol. 57, no. 2, pp. 138–144, 2019.
- [5] G. P. Fettweis, "The Tactile Internet: applications & challenges," *IEEE Veh. Technol. Mag.*, vol. 9, no. 1, pp. 64–70, Mar. 2014.
- [6] 3GPP TR 38.802 V2.0.0, "Study on new radio (NR) access technology; physical layer aspects (release 14)," 2017.
- [7] C. She, C. Yang, and T. Q. S. Quek, "Radio resource management for ultra-reliable and low-latency communications," *IEEE Commun. Mag.*, vol. 55, no. 6, pp. 72–78, 2017.
- [8] T. K. Vu, C.-F. Liu, M. Bennis *et al.*, "Ultra-reliable and low latency communication in mmwave-enabled massive MIMO networks," *IEEE Commun. Letters*, vol. 21, no. 9, pp. 2041–2044, Sep. 2017.
- [9] J. J. Nielsen, R. Liu, and P. Popovski, "Ultra-reliable low latency communication using interface diversity," *IEEE Trans. on Commun.*, vol. 66, no. 3, pp. 1322–1334, Mar. 2018.
- [10] X. Lin, J. Li, R. Baldemair *et al.*, "5G New Radio: unveiling the essentials of the next generation wireless access technology," 2018. [Online]. Available: <https://arxiv.org/abs/1806.06898>
- [11] P. Schulz, M. Matthe, H. Klessig *et al.*, "Latency critical IoT applications in 5G: Perspective on the design of radio interface and network architecture," *IEEE Commun. Mag.*, vol. 55, no. 2, pp. 70–78, 2017.
- [12] T. Jacobsen, R. Abreu, G. Berardinelli *et al.*, "System level analysis of uplink grant-free transmission for URLLC," in *Proc. IEEE Globecom Workshops*, 2017, pp. 1–6.
- [13] B. Soret, P. Mogensen, K. I. Pedersen, and M. C. Aguayo-Torres, "Fundamental tradeoffs among reliability, latency and throughput in cellular networks," in *Proc. IEEE Globecom Workshops*, 2014, pp. 1391–1396.
- [14] J. Sachs, G. Wikstrom, T. Dudda *et al.*, "5G radio network design for ultra-reliable low-latency communication," *IEEE Network*, vol. 32, no. 2, pp. 24–31, 2018.

- [15] W. Yang, G. Durisi, T. Koch, and Y. Polyanskiy, “Quasi-static multiple-antenna fading channels at finite blocklength,” *IEEE Trans. Inf. Theory*, vol. 60, no. 7, pp. 4232–4265, Jul. 2014.
- [16] M. Bennis, M. Debbah, and H. V. Poor, “Ultra-reliable and low-latency wireless communication: Tail, risk and scale,” *arXiv preprint arXiv:1801.01270*, 2018.
- [17] C. She, C. Yang, and T. Q. S. Quek, “Cross-layer optimization for ultra-reliable and low-latency radio access networks,” *IEEE Wireless Commun.*, vol. 17, no. 1, pp. 127–141, 2018.
- [18] G. Berardinelli, N. H. Mahmood, R. Abreu, T. Jacobsen, K. Pedersen, I. Z. Kovács, and P. Mogensen, “Reliability analysis of uplink grant-free transmission over shared resources,” *IEEE Access*, vol. 6, pp. 23 602–23 611, 2018.
- [19] X. Tong, G. Zhao, M. A. Imran *et al.*, “Minimizing wireless resource consumption for packetized predictive control in real-time cyber physical systems,” in *Proc. IEEE ICC Workshops*, May 2018.
- [20] M. Simsek, A. Aijaz, M. Dohler, J. Sachs, and G. Fettweis, “5G-enabled tactile internet,” *IEEE J. Sel. Areas Commun.*, vol. 34, no. 3, pp. 460–473, Mar. 2016.
- [21] Z. Hou, C. She, Y. Li *et al.*, “Burstiness aware bandwidth reservation for ultra-reliable and low-latency communications (URLLC) in Tactile Internet,” *IEEE J. Sel. Areas Commun.*, vol. 36, no. 11, pp. 2401–2410, 2018.
- [22] M. Li, X. Guan, C. Hua, C. Chen, and L. Lyu, “Predictive pre-allocation for low-latency uplink access in industrial wireless networks,” in *Proc. IEEE INFOCOM*, 2018, pp. 306–314.
- [23] B. Makki, T. Svensson, G. Caire, and M. Zorzi, “Fast HARQ over finite blocklength codes: A technique for low-latency reliable communication,” *IEEE Wireless Commun.*, vol. 18, no. 1, pp. 194–209, 2018.
- [24] N. Strodthoff, B. Göktepe, T. Schierl *et al.*, “Enhanced machine learning techniques for early HARQ feedback prediction in 5G,” *arXiv preprint arXiv:1807.10495*, 2018.
- [25] C. She, Y. Duan, G. Zhao, T. Q. S. Quek, Y. Li, and B. Vucetic, “Cross-layer design for mission-critical IoT in mobile edge computing systems,” *IEEE Internet of Things J.*, *early access*, 2019.
- [26] S. Feyzabadi, S. Straube, M. Folgheraiter *et al.*, “Human force discrimination during active arm motion for force feedback design,” *IEEE Trans. Haptics*, vol. 6, no. 3, pp. 309–319, 2013.
- [27] S. M. Kay, *Fundamentals of statistical signal processing, volume I: estimation theory*. Prentice Hall, 1993.
- [28] G. Klančar and I. Škrjanc, “Tracking-error model-based predictive control for mobile robots in real time,” *Robotics and autonomous systems*, vol. 55, no. 6, pp. 460–469, 2007.
- [29] C.-S. Chang and J. A. Thomas, “Effective bandwidth in high-speed digital networks,” *IEEE J. Sel. Areas Commun.*, vol. 13, no. 6, pp. 1091–1100, 1995.
- [30] H. Al-Zubaidy, J. Liebeherr, and A. Burchard, “Network-layer performance analysis of multihop fading channels,” *IEEE/ACM Trans. Netw.*, vol. 24, no. 1, pp. 204–217, Feb. 2016.
- [31] M. Condoluci, T. Mahmoodi, E. Steinbach, and M. Dohler, “Soft resource reservation for low-delayed teleoperation over mobile networks,” *IEEE Access*, vol. 5, pp. 10 445–10 455, May 2017.
- [32] S. Schiessl, H. Al-Zubaidy, M. Skoglund, and J. Gross, “Delay performance of wireless communications with imperfect CSI and finite-length coding,” *IEEE Trans. Commun.*, vol. 66, no. 12, pp. 6527–6541, 2018.
- [33] J. Östman, G. Durisi, E. G. Ström, M. C. Coşkun, and G. Liva, “Short packets over block-memoryless fading channels: Pilot-assisted or noncoherent transmission?” *IEEE Trans. Commun.*, vol. 67, no. 2, pp. 1521–1536, 2018.
- [34] M. Mousaei and B. Smida, “Optimizing pilot overhead for ultra-reliable short-packet transmission,” in *Proc. IEEE ICC*, 2017, pp. 1–5.
- [35] B. Hassibi and B. M. Hochwald, “How much training is needed in multiple-antenna wireless links?” *IEEE Trans. Inf. Theory*, vol. 49, no. 4, pp. 951–963, 2003.

- [36] A. Lancho, J. Ostman, G. Durisi *et al.*, “Saddlepoint approximations for Rayleigh block-fading channels,” 2019. [Online]. Available: <https://arxiv.org/abs/1904.10442>
- [37] M. Shirvanimoghaddam, M. S. Mohammadi, R. Abbas *et al.*, “Short block-length codes for ultra-reliable low latency communications,” *IEEE Commun. Mag.*, vol. 57, no. 2, pp. 130–137, 2018.
- [38] S. Schiessl, J. Gross, and H. Al-Zubaidy, “Delay analysis for wireless fading channels with finite blocklength channel coding,” in *Proc. ACM MSWiM*, 2015, pp. 13–22.
- [39] C. She, Z. Chen, C. Yang *et al.*, “Improving network availability of ultra-reliable and low-latency communications with multi-connectivity,” *IEEE Trans. Commun.*, vol. 66, no. 11, pp. 5482–5496, Nov. 2018.
- [40] J. Mathews and K. Fink, *Numerical methods using MATLAB*. Pearson Prentice Hall, NJ, 2004.